Studies on quark-mass dependence of the $N^*(920)$ pole from πN χPT amplitudes

Kai-Ge Kang[1,2]*, Xu Wang[2]†, Qu-Zhi Li[1]‡, Zhiguang Xiao[1]§and Han-Qing Zheng[1]¶

[1] Institute of Particle and Nuclear Physics, Sichuan University, Chengdu, Sichuan 610065, China

[2] School of Physics, Peking University, Beijing 100871, China

May 18, 2025

Abstract

The quark-mass dependence of the $N^*(920)$ resonance is analyzed on K-matrix with the πN scattering amplitude calculated up to next-to-next-to-leading order in chiral perturbation theory. As the quark mass increases, $N^*(920)$ moves to the positive real axis in the complex energy s plane. Finally, it tends to drop into the u channel cut when the pion mass become 420 MeV.

The study of pion-nucleon scatterings has a history over sixty years. It is a surprise that only till very recently the pole structure of the pion N scattering amplitude below threshold, especially in the S_{11} channel, has been made clear. [1–4] In these studies, dispersion techniques play a crucial role, [5, 6], aided by unitarity constraint, i.e., the production representation [7–11]. As a result, a novel subthreshold pole in S_{11} channel located at $\sqrt{s} = (918 \pm 3) - i(163 \pm 9)$ GeV was established (see also Ref. [12]), and the existence of such a subthreshold pole has also been confirmed by K-matrix fit [13] and N/D method [14].

On the other side, the quark-mass dependence of resonance poles is an important subject since it is connected with the lattice studies on low energy QCD, providing a special angle for investigating strong interaction physics. This exercise has been applied to the prominent σ pole trajectory [15–18]. The first attempt to study the $N^*(920)$ trajectory with varying pion masses was carried out in a linear sigma model with nucleons in Ref. [19]. The main reason in Ref. [19] to choose the linear realization of chiral symmetry is to keep a better symmetry property at high temperatures. Since chiral perturbation theory provides a more general frame to parametrize our ignorance, i.e., the non-renormalizable terms, here we will choose chiral lagrangians with baryons to study the trajectory with varying quark mass, or the pion mass.

The partial wave πN scattering amplitude in LS scheme, denoted as T [1], satisfies the partial wave optical theorem:

$$\mathrm{Im}\, T(s) = \rho(s)|T(s)|^2 \ . \tag{1}$$

The partial wave S matrix element in S_{11} channel can be defined as

$$S = 1 + 2i\rho(s)T \ , \tag{2}$$

where $\rho(s) = \sqrt{[s - (m_N + M_\pi)^2][s - (m_N - M_\pi)^2]}/s$. A K-matrix approximation is used to restore unitarity from perturbation amplitudes. The partial wave amplitude and partial wave S matrix element are

$$\tilde{T} = \frac{K}{1 - i\rho K},\ \tilde{S} = \frac{1 + i\rho K}{1 - i\rho K} \ . \tag{3}$$

Usually K is taken as the real part of the perturbation amplitude. For πN scattering, it is $\mathcal{K}^{(2)} \equiv T^{(2)}$ for $\mathcal{O}(p^2)$ calculation, and $\mathcal{K}^{(3)} \equiv T^{(3)} - i\rho(T^{(1)})^2$ for $\mathcal{O}(p^3)$ calculation.

The partial wave amplitude as constructed is a real analytical function in the complex s plane. There exists a physical cut, or right-hand cut, above the threshold $s > (m_N + M_\pi)^2$. Partial wave projection and loop integrals will also introduce other cuts, called left-hand cuts. All the cut structures in πN scattering are shown in Fig. 1 [6, 20]. However, in general, such unitarization approximations suffer from problems of violation of

*kaige@stu.pku.edu.cn; part of this work is done while the author was visiting SCU.

†wangxu0604@stu.pku.edu.cn

‡liqz@scu.edu.cn (corresponding author)

§xiaozg@scu.edu.cn (corresponding author)

¶zhenghq@scu.edu.cn

[1] The process of partial wave projection is standard, see for example, Ref. [1].

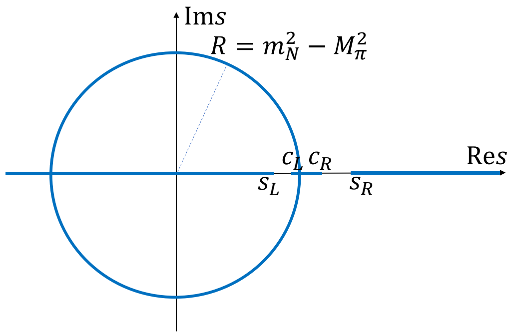

Figure 1: Cuts in πN scattering partial wave $\mathcal{S}$ matrix element, represented by the bold lines. $s_L = (m_N - M_\pi)^2, c_L = (m_N^2 - M_\pi^2)^2/m_N^2, c_R = m_N^2 + 2M_\pi^2, s_R = (m_N + M_\pi)^2$

analyticity and crossing symmetry [21–24].[2] A direct consequence is the appearance of spurious physical sheet resonances (SPSRs). A case by case analysis seems to be required, at least, to ensure that the SPSRs play a minor contribution to physical quantities such as phase shifts. Barring for this, the K-matrix unitarization provides a quick but rough estimates of the physical pole position such as $N^*(920)$.

To proceed, we follow Refs. [1,25]. Firstly we repeated the $O(p^2)$ and $O(p^3)$ results of Ref. [25]. The obtained partial wave unitary amplitude can be used to calculate the corresponding phase shift $\delta = \arctan[\rho\tilde{T}]$ and fit to the phase shift data which in turn determine the low energy constants. We directly use the results in Ref. [1]:

$$c_1 = -0.841\ \text{GeV}^{-1},\ c_2 = -1.170\ \text{GeV}^{-1},\ c_3 = -2.618\ \text{GeV}^{-1},\ c_4 = -1.677\ \text{GeV}^{-1}\ . \tag{4}$$

Substituting these low energy constants and physical quantities $m_N = 0.9383$ GeV, $M = 0.1396$ GeV, $F_\pi = 0.0924$ GeV, $g_A = 1.267$, we can calculate the cuts and poles of the partial wave unitary matrix element of the S_{11} channel on the complex s plane. Results are shown in Table 1. The pole corresponding to $N^*(920)$ resonance is $\sqrt{s} = 0.9541 \pm i0.2653$ GeV. The specific positions of some poles including $N^*(920)$ are shown in Figure 4(a).

Analytic structures	Resonances	virtual states
pole positions (GeV)	$0.9541 \pm i0.2653$	0.9174, 0.9590

Table 1: The pole positions in the $\mathcal{O}(p^2)$ πN scattering matrix element processed by K-matrix unitarization.

In the isospin limit, pion mass is related to quark mass by $M_\pi^2 \propto 2B_0\hat{m}$ with $\hat{m} = (m_u + m_d)/2$ [26]. Therefore, studying the quark-mass dependence of $N^*(920)$ is equivalent to studying its changes with the increase of the pion mass. In addition, we also need to know the values of physical quantities such as m_N, g_A, and F_π at different pion masses. Some results have been given by the lattice QCD calculation, and there are also some theoretical fits on these results. For m_N, we use the ruler approximation in Ref. [27], that is, $m_N = 800$ MeV $+ M_\pi$, which is consistent with the lattice QCD results [28] in a large range. For g_A, we use the $\mathcal{O}(p^3)$ result in Ref. [29], and for F_π, we use the fit result with strategy 2 in Ref. [30]. Substituting these results into the partial wave unitary matrix element, we finally get the $N^*(920)$ trajectory when the pion mass increases from 0.1396 GeV to 0.44 GeV, as shown in Figure 2. Pole positions with different pion masses are plotted in Figure 4, where $N^*(920)$ pole locates at $\sqrt{s} = 1.1157 \pm i0.1534$ GeV for $M_\pi = 300$MeV, and $\sqrt{s} = 1.2154 \pm i0.0318$ GeV for $M_\pi = 440$MeV, respectively. As can be seen from Figure 2, the $N^*(920)$ pole gradually falls down to the real axis. When the pion mass reaches 0.44 GeV, the pole is very close to the real axis and is still above the u cut. It can be inferred that if the pion mass increases further, the pole will fall into the u cut.

One can also go to the $\mathcal{K}^{(3)}$ approximation to check the stability of our approximation. Remember that $\mathcal{K}^{(3)} = T^{(3)} - i\rho(T^{(1)})^2$, we need more low energy constants comparing with $\mathcal{K}^{(2)}$. we use the results of Fit 1 in Ref. [31]:

$$\begin{aligned} &c_1 = -1.22\text{GeV}^{-1},\ c_2 = 3.58\text{GeV}^{-1},\ c_3 = -6.04\text{GeV}^{-1},\ c_4 = 3.48\text{GeV}^{-1} \\ &d_1 + d_2 = 3.25\text{GeV}^{-2},\ d_3 = -2.88\text{GeV}^{-2},\ d_5 = -0.15\text{GeV}^{-2}, \\ &d_{14} - d_{15} = -6.19\text{GeV}^{-2},\ d_{18} = -1.07\text{GeV}^{-2} \end{aligned} \tag{5}$$

Substituting these low energy constants, we can find the pole distribution of the partial wave unitary matrix elements for $M_\pi = 139.6$ MeV, 300 MeV and 420 MeV, as shown in sub-figures (b), (d), and (f) of Figure 4.

[2] For example, a [1,1] Padé approximant of π scattering tend to put all contributions from different sources, e.g., s channel poles, left hand cuts, crossed channel resonance exchanges, into one single s channel resonance.

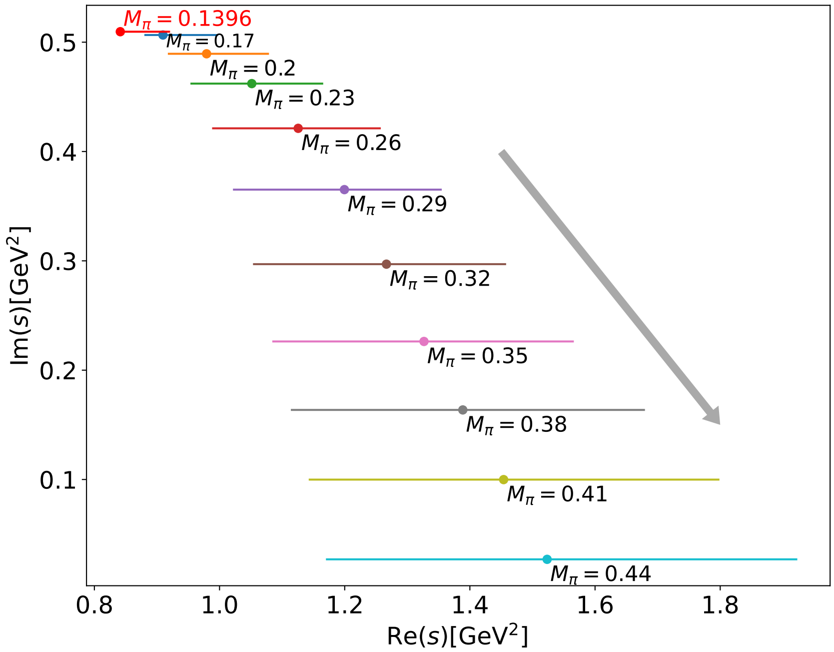

Figure 2: Variation of $N^*(920)$ pole position with the pion mass in $\mathcal{K}_2$ amplitude. The unit is GeV. The horizontal line segment shifted downward to the horizontal axis is the position of the u cut at the corresponding pion mass. The dot represents the position of $N^*(920)$ at the corresponding pion mass.

The corresponding positions of $N^*(920)$ pole are $\sqrt{s} = 0.8897 \pm i0.2633$ GeV, $\sqrt{s} = 1.1157 \pm i0.1534$ GeV and $\sqrt{s} = 1.2154 \pm i0.0318$ GeV, respectively. Specifically, as the pion mass increases from 0.1396 GeV to 0.42 GeV, the trajectory of $N^*(920)$ is shown in Figure 3.

From Figure 4, we can see that the position of the poles far from the threshold are very different from the result of $\mathcal{O}(p^2)$, while the position of $N^*(920)$ pole does not change much. From Figure 3, we can see that even though considering the $\mathcal{O}(p^3)$ contribution, as the pion mass increases, $N^*(920)$ will still fall into the u cut.

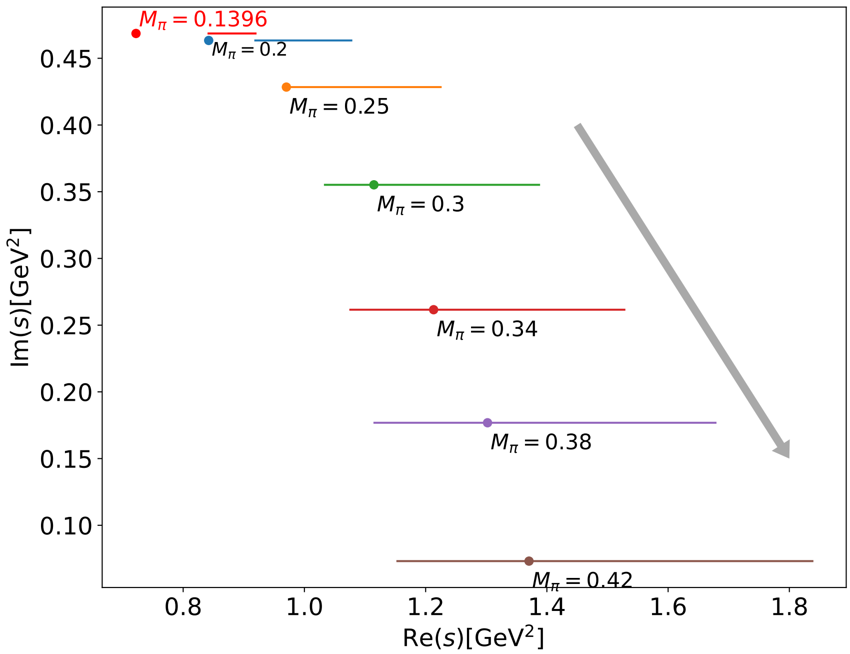

Figure 3: The $N^*(920)$ pole trajectory with varying pion masses obtained by combining the $\mathcal{O}(p^3)$ ChPT amplitude with the K-matrix unitarization.

discussion

Acknowlegement: This work is supported by China National Natural Science Foundation under Contract No. 12335002, 12375078. This work is also supported by "the Fundamental Research Funds for the Central

Universities".

References

[1] Y.-F. Wang, D.-L. Yao, and H.-Q. Zheng, "New Insights on Low Energy πN Scattering Amplitudes," *Eur. Phys. J. C* **78** no. 7, (2018) 543, arXiv:1712.09257 [hep-ph].

[2] Y.-F. Wang, D.-L. Yao, and H.-Q. Zheng, "New insights on low energy πN scattering amplitudes: comprehensive analyses at $\mathcal{O}(p^3)$ level," *Chin. Phys. C* **43** no. 6, (2019) 064110, arXiv:1811.09748 [hep-ph].

[3] Q.-Z. Li and H.-Q. Zheng, "Singularities and accumulation of singularities of πN scattering amplitudes," *Commun. Theor. Phys.* **74** no. 11, (2022) 115203, arXiv:2108.03734 [nucl-th].

[4] X.-H. Cao, Q.-Z. Li, and H.-Q. Zheng, "A possible subthreshold pole in S_{11} channel from πN Roy-Steiner equation analyses," *JHEP* **12** (2022) 073, arXiv:2207.09743 [hep-ph].

[5] G. E. Hite and F. Steiner, "New dispersion relations and their application to partial-wave amplitudes," *Nuovo Cim. A* **18** (1973) 237–270.

[6] J. Kennedy and T. D. Spearman, "Singularities in Partial-Wave Amplitudes for Two Ingoing and Two Outgoing Particles," *Phys. Rev.* **126** no. 4, (1962) 1596–1602.

[7] H. Q. Zheng, Z. Y. Zhou, G. Y. Qin, Z. Xiao, J. J. Wang, and N. Wu, "The kappa resonance in s wave pi K scatterings," *Nucl. Phys. A* **733** (2004) 235–261, arXiv:hep-ph/0310293.

[8] Z. Y. Zhou, G. Y. Qin, P. Zhang, Z. Xiao, H. Q. Zheng, and N. Wu, "The Pole structure of the unitary, crossing symmetric low energy pi pi scattering amplitudes," *JHEP* **02** (2005) 043, arXiv:hep-ph/0406271.

[9] Z. Y. Zhou and H. Q. Zheng, "An improved study of the kappa resonance and the non-exotic s wave πK scatterings up to $\sqrt{s} = 2.1$GeV of LASS data," *Nucl. Phys. A* **775** (2006) 212–223, arXiv:hep-ph/0603062.

[10] Z. Xiao and H. Q. Zheng, "Left-hand singularities, hadron form-factors and the properties of the sigma meson," *Nucl. Phys. A* **695** (2001) 273–294, arXiv:hep-ph/0011260.

[11] J. He, Z. Xiao, and H. Q. Zheng, "The Constraints of unitary on $\pi\pi$ scattering dispersion relations," *Phys. Lett. B* **536** (2002) 59–66, arXiv:hep-ph/0201257. [Erratum: Phys.Lett.B 549, 362–363 (2002)].

[12] M. Hoferichter, J. R. de Elvira, B. Kubis, and U.-G. Meißner, "Nucleon resonance parameters from Roy–Steiner equations," *Phys. Lett. B* **853** (2024) 138698, arXiv:2312.15015 [hep-ph].

[13] Y. Ma, W.-Q. Niu, Y.-F. Wang, and H.-Q. Zheng, "How does the S_{11} $N^*(890)$ state emerge from a naive K-matrix fit?," *Commun. Theor. Phys.* **72** no. 10, (2020) 105203, arXiv:2002.02351 [hep-ph].

[14] Q.-Z. Li, Y. Ma, W.-Q. Niu, Y.-F. Wang, and H.-Q. Zheng, "An N/D study of the S11 channel πN scattering amplitude," *Chin. Phys. C* **46** no. 2, (2022) 023104, arXiv:2102.00977 [nucl-th].

[15] X.-H. Cao, Q.-Z. Li, Z.-H. Guo, and H.-Q. Zheng, "Roy equation analyses of $\pi\pi$ scatterings at unphysical pion masses," *Phys. Rev. D* **108** no. 3, (2023) 034009, arXiv:2303.02596 [hep-ph].

[16] Y.-L. Lyu, Q.-Z. Li, Z. Xiao, and H.-Q. Zheng, "Revisiting O(N) σ model at unphysical pion masses and high temperatures. II. The vacuum structure and thermal σ pole trajectory with cross-channel improvements," *Phys. Rev. D* **110** no. 9, (2024) 094054, arXiv:2405.11313 [hep-ph].

[17] Y.-L. Lyu, Q.-Z. Li, Z. Xiao, and H.-Q. Zheng, "Revisiting O(N) σ model at unphysical pion masses and high temperatures," *Phys. Rev. D* **109** no. 9, (2024) 094026, arXiv:2402.19243 [hep-ph].

[18] C. Hanhart, J. R. Pelaez, and G. Rios, "Quark mass dependence of the rho and sigma from dispersion relations and Chiral Perturbation Theory," *Phys. Rev. Lett.* **100** (2008) 152001, arXiv:0801.2871 [hep-ph].

[19] Q.-Z. Li, Z. Xiao, and H.-Q. Zheng, "On the pole trajectory of the subthreshold negative parity nucleon with varying pion masses," arXiv:2501.01619 [hep-ph].

[20] S. W. MacDowell, “Analytic Properties of Partial Amplitudes in Meson-Nucleon Scattering,” *Phys. Rev.* **116** (1959) 774–778.

[21] G.-Y. Qin, W. Z. Deng, Z. Xiao, and H. Q. Zheng, “The [1,2] Pade amplitudes for pi pi scatterings in chiral perturbation theory,” *Phys. Lett. B* **542** (2002) 89–99, `arXiv:hep-ph/0205214`.

[22] Z. H. Guo, J. J. Sanz Cillero, and H. Q. Zheng, “Partial waves and large N(C) resonance sum rules,” *JHEP* **06** (2007) 030, `arXiv:hep-ph/0701232`.

[23] Z. H. Guo, J. J. Sanz-Cillero, and H. Q. Zheng, “O(p**6) extension of the large - N(C) partial wave dispersion relations,” *Phys. Lett. B* **661** (2008) 342–347, `arXiv:0710.2163 [hep-ph]`.

[24] D.-L. Yao, L.-Y. Dai, H.-Q. Zheng, and Z.-Y. Zhou, “A review on partial-wave dynamics with chiral effective field theory and dispersion relation,” *Rept. Prog. Phys.* **84** no. 7, (2021) 076201, `arXiv:2009.13495 [hep-ph]`.

[25] Y.-H. Chen, D.-L. Yao, and H. Q. Zheng, “Analyses of pion-nucleon elastic scattering amplitudes up to $O(p^4)$ in extended-on-mass-shell subtraction scheme,” *Phys. Rev. D* **87** (2013) 054019, `arXiv:1212.1893 [hep-ph]`.

[26] M. Gell-Mann, R. J. Oakes, and B. Renner, “Behavior of current divergences under SU(3) x SU(3),” *Phys. Rev.* **175** (1968) 2195–2199.

[27] A. Walker-Loud, “Nuclear Physics Review,” *PoS* **LATTICE2013** (2014) 013, `arXiv:1401.8259 [hep-lat]`.

[28] **XQCD** Collaboration, M. Gong *et al.*, “Strangeness and charmness content of the nucleon from overlap fermions on 2+1-flavor domain-wall fermion configurations,” *Phys. Rev. D* **88** (2013) 014503, `arXiv:1304.1194 [hep-ph]`.

[29] F. Alvarado and L. Alvarez-Ruso, “Light-quark mass dependence of the nucleon axial charge and pion-nucleon scattering phenomenology,” *Phys. Rev. D* **105** no. 7, (2022) 074001, `arXiv:2112.14076 [hep-ph]`.

[30] M. Niehus, M. Hoferichter, B. Kubis, and J. Ruiz de Elvira, “Two-Loop Analysis of the Pion Mass Dependence of the ρ Meson,” *Phys. Rev. Lett.* **126** no. 10, (2021) 102002, `arXiv:2009.04479 [hep-ph]`.

[31] D.-L. Yao, D. Siemens, V. Bernard, E. Epelbaum, A. M. Gasparyan, J. Gegelia, H. Krebs, and U.-G. Meißner, “Pion-nucleon scattering in covariant baryon chiral perturbation theory with explicit Delta resonances,” *JHEP* **05** (2016) 038, `arXiv:1603.03638 [hep-ph]`.

[32] Y.-F. Wang, D.-L. Yao, and H.-Q. Zheng, “New insights on low energy πn scattering amplitudes,” *The European Physical Journal C* **78** no. 7, (July, 2018) . `http://dx.doi.org/10.1140/epjc/s10052-018-6024-5`.

[33] D. Siemens, V. Bernard, E. Epelbaum, A. M. Gasparyan, H. Krebs, and U.-G. Meißner, “Elastic and inelastic pion-nucleon scattering to fourth order in chiral perturbation theory,” *Physical Review C* **96** no. 5, (Nov., 2017) . `http://dx.doi.org/10.1103/PhysRevC.96.055205`.

[34] J.-M. Chen, Z.-R. Liang, and D.-L. Yao, “Low-energy elastic (anti)neutrino-nucleon scattering in covariant baryon chiral perturbation theory,” 2024. `https://arxiv.org/abs/2403.17743`.

[35] J. Bijnens, “Chiral perturbation theory and mesons,” 2013. `https://arxiv.org/abs/1301.6953`.

[36] Y.-H. Chen, D.-L. Yao, and H. Q. Zheng, “Analyses of pion-nucleon elastic scattering amplitudes up to $o(p^4)$ in extended-on-mass-shell subtraction scheme,” 2012. `https://arxiv.org/abs/1212.1893`.

A Running results of the $N^*(920)$ in ChPT

In addition to the dependencies provided by lattice QCD, we can also obtain the m_N, F_π and g_A dependencies on M_π from chiral perturbation theory. The relations are as follows:

$$
\begin{aligned}
m_N &= m - 4c_1 M^2 + \Delta_m, \Delta_m = \frac{3g^2 m_N}{32\pi^2 F^2} \times [A_0(m_N^2) + M^2 B_0(m_N^2, M^2, m_N^2)], \\
F_\pi &= F + \Delta_F, \Delta_F = \frac{l_4 M^2}{F} + \frac{A_0[M^2]}{16\pi^2 F}, l_4 = l_4^r + \gamma_4 \lambda, \\
\lambda &= \frac{1}{(4\pi)^2}\mu^{d-4}\left\{\frac{1}{d-4} - \frac{1}{2}(\ln 4\pi + \Gamma'(1) + 1)\right\}, l_4^r = \frac{\gamma_4}{32\pi^2}\left(\bar{l}_4 + \ln\frac{M^2}{\mu^2}\right), \quad \gamma_4 = 2, \\
g_A &= g + 4d_{16}M^2 + \Delta_g, \\
\Delta_g &= \frac{g[4(g^2-2)m_N^2 + (3g^2+2)M^2]}{16\pi^2 F^2(4m_N^2 - M^2)} A_0[m_N^2] + \frac{g[(8g^2+4)m_N^2 - (4g^2+1)M^2]}{16\pi^2 F^2(4m_N^2 - M^2)} \\
&\quad + \frac{gM^2[-8(g^2+1)m_N^2 + (3g^2+2)M^2]}{16\pi^2 F^2(4m_N^2 - M^2)} B_0[m_N^2, m_N^2, M^2] - \frac{g^3 m_N^2(4m_N^2 + 3M^2)}{16\pi^2 F^2(4m_N^2 - M^2)}
\end{aligned} \tag{6}
$$

where A_0 and B_0 are Passarino-Veltman functions.

In the $\mathcal{O}(p^2)$ calculations, since loop diagrams are not involved, the above expressions can be significantly simplified.

We first choose the parameters [32]:

$$
c_1 = -0.841\,\mathrm{GeV}^{-1}, \quad c_2 = 1.17\,\mathrm{GeV}^{-1}, \quad c_3 = -2.618\,\mathrm{GeV}^{-1}, \quad c_4 = 1.677\,\mathrm{GeV}^{-1} \tag{7}
$$

The resulting trajectory of the $N^*(920)$ pole is shown in Fig. 5

Figure 5 shows the trajectory of $N^*(920)$ in the s-plane. As the pion mass increases, the $N^*(920)$ pole moves toward the real axis and eventually falls onto the u-channel cut.

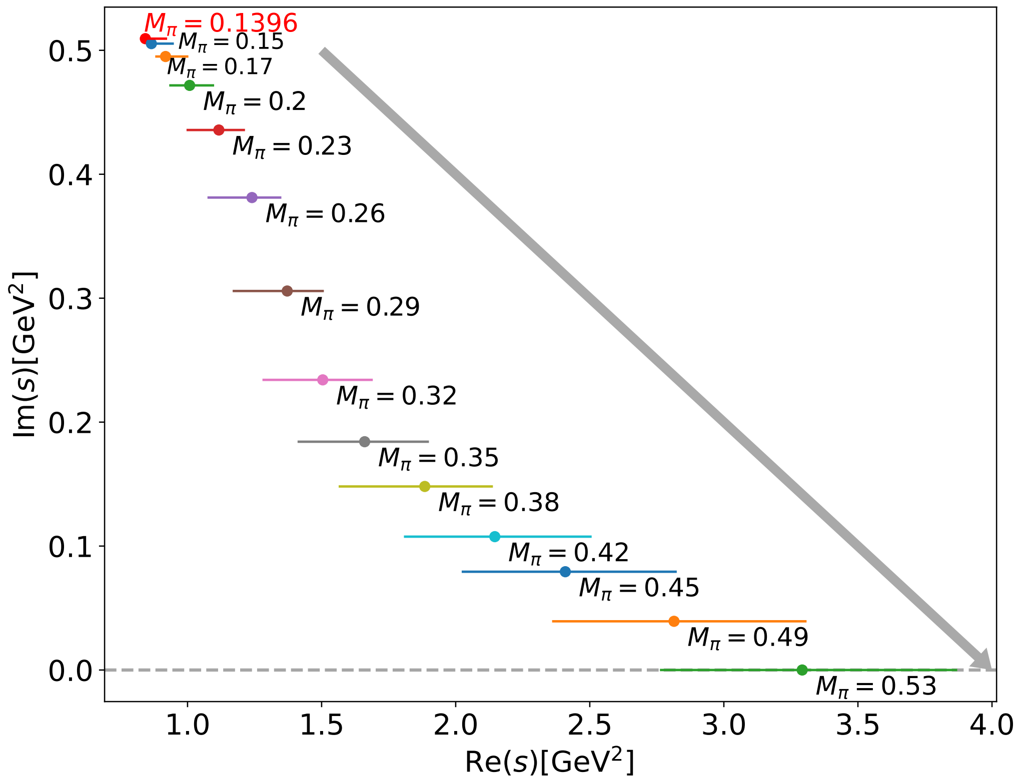

Figure 5: Trajectory of $N^*(920)$ pole in s-plane at $\mathcal{O}(p^2)$

In addition, we examined another set of parameters [33]:

$$
c_1 = -2.12\,\mathrm{GeV}^{-1}, \quad c_2 = 2.65\,\mathrm{GeV}^{-1}, \quad c_3 = -6.28\,\mathrm{GeV}^{-1}, \quad c_4 = 4.32\,\mathrm{GeV}^{-1} \tag{8}
$$

The results are shown in Fig. 6. While both parameter sets lead to the same qualitative conclusion (the pole eventually falls onto the u-channel cut), they exhibit different rates of descent toward the real axis.

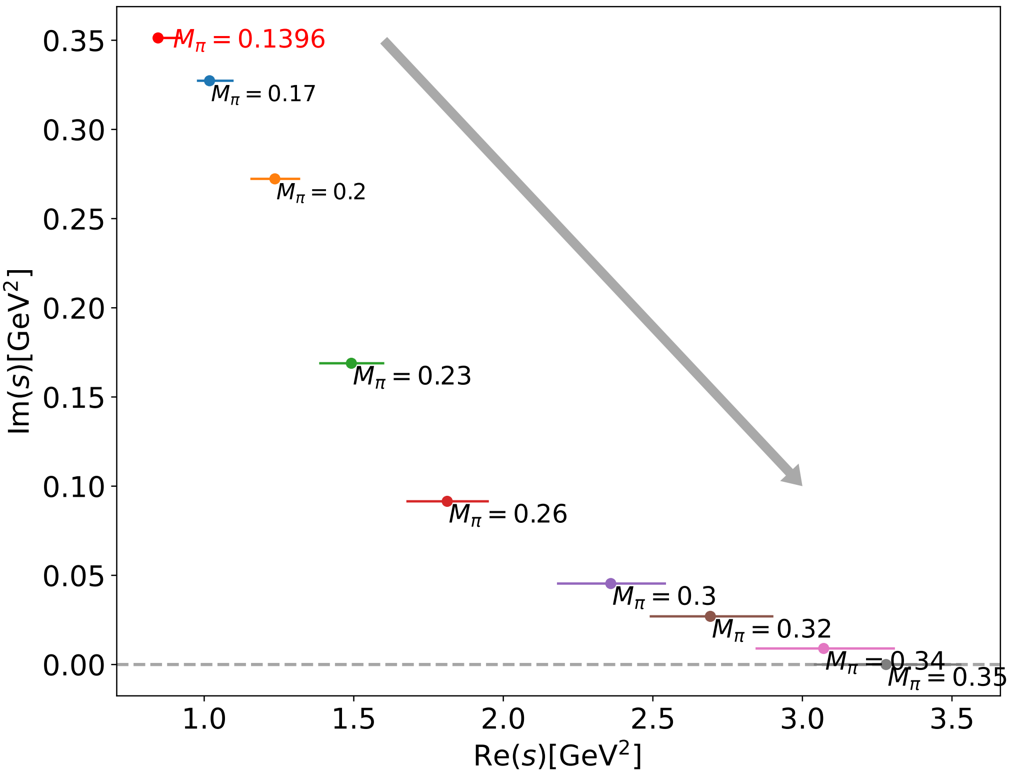

Figure 6: Trajectory of $N^*(920)$ pole in s-plane at $\mathcal{O}(p^2)$

Furthermore, we extended our analysis to $\mathcal{O}(p^3)$ calculations. Using Eqs. (6) we plotted their dependence on the pion mass M_π as follows. Here we have chosen the following parameter values: $c_1 = -1.22\,\mathrm{GeV}^{-1}$ [31], $d_{16} = -0.83\,\mathrm{GeV}^{-2}$ [34], and $\bar{l}_4 = 4.4$ [35].

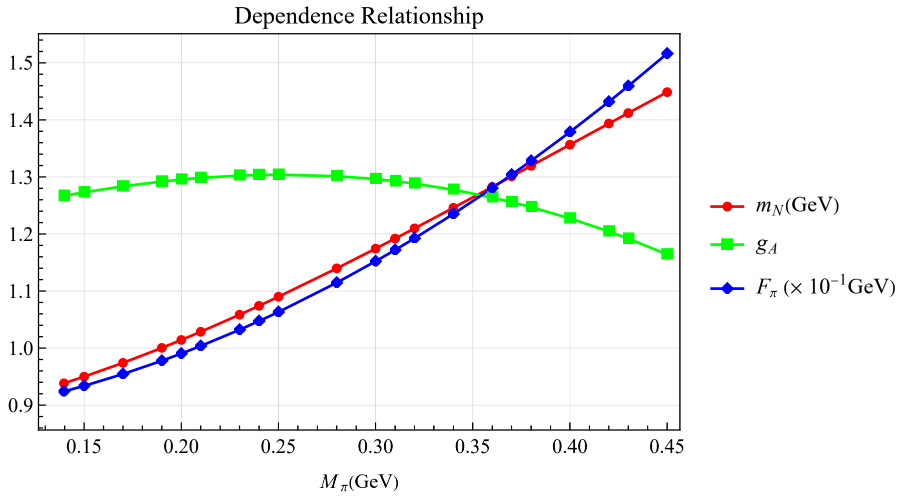

Figure 7: Dependencies of m_N, g_A and F_π on the pion mass M_π

For the $\mathcal{O}(p^3)$ tree-level calculations, we employed the following parameter set [31]:

$$
\begin{aligned}
&c_1 = -1.22\,\mathrm{GeV}^{-1}, \quad c_2 = 3.58\,\mathrm{GeV}^{-1}, \quad c_3 = -6.04\,\mathrm{GeV}^{-1}, \quad c_4 = 3.48\,\mathrm{GeV}^{-1} \\
&d_{1+2} = 3.25\,\mathrm{GeV}^{-2}, \quad d_3 = -2.88\,\mathrm{GeV}^{-2}, \quad d_5 = -0.15\,\mathrm{GeV}^{-2} \\
&d_{14-15} = -6.19\,\mathrm{GeV}^{-2}, \quad d_{18} = -1.07\,\mathrm{GeV}^{-2}
\end{aligned}
\tag{9}
$$

The tree-level results at $\mathcal{O}(p^3)$ are presented in Fig. 8:

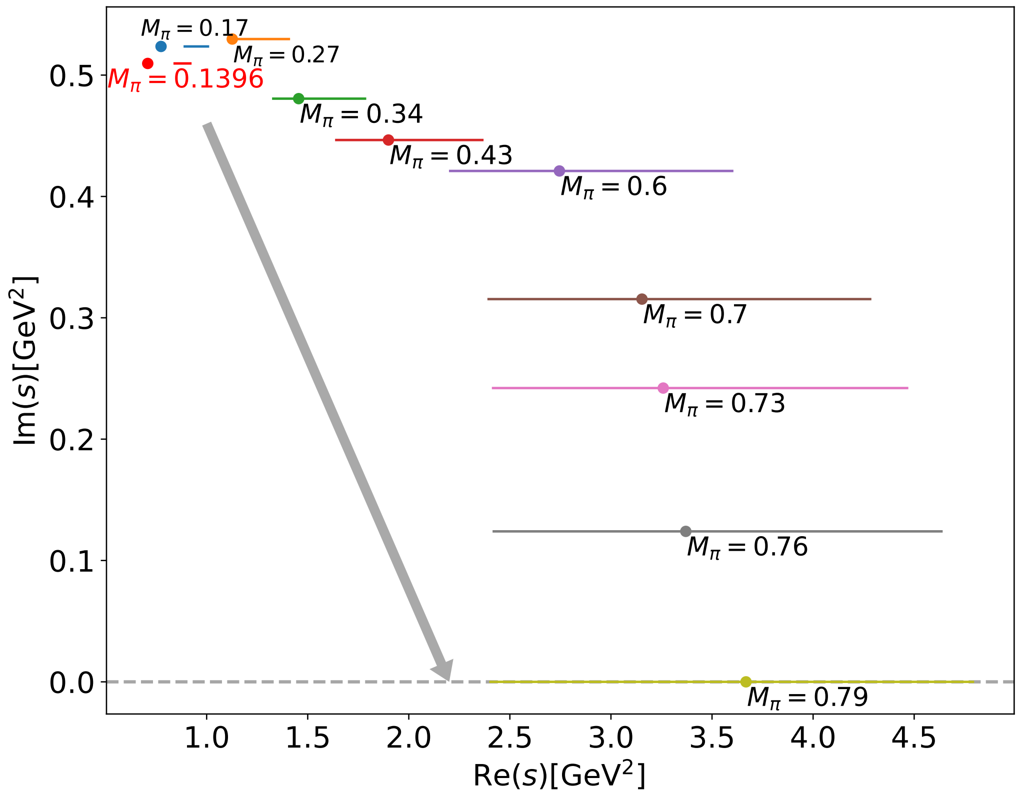

Figure 8: Trajectory of $N^*(920)$ pole in s-plane at $\mathcal{O}(p^3)$

Using an alternative parameter set [36],

$$\begin{aligned}
c_1 &= -1.39\,\mathrm{GeV}^{-1}, \quad c_2 = 4.01\,\mathrm{GeV}^{-1}, \quad c_3 = -6.61\,\mathrm{GeV}^{-1}, \quad c_4 = 3.92\,\mathrm{GeV}^{-1}\\
d_{1+2} &= 4.40\,\mathrm{GeV}^{-2}, \quad d_3 = -3.02\,\mathrm{GeV}^{-2}, \quad d_5 = -0.62\,\mathrm{GeV}^{-2}\\
d_{14-15} &= -7.15\,\mathrm{GeV}^{-2}, \quad d_{18} = -0.56\,\mathrm{GeV}^{-2}
\end{aligned} \tag{10}$$

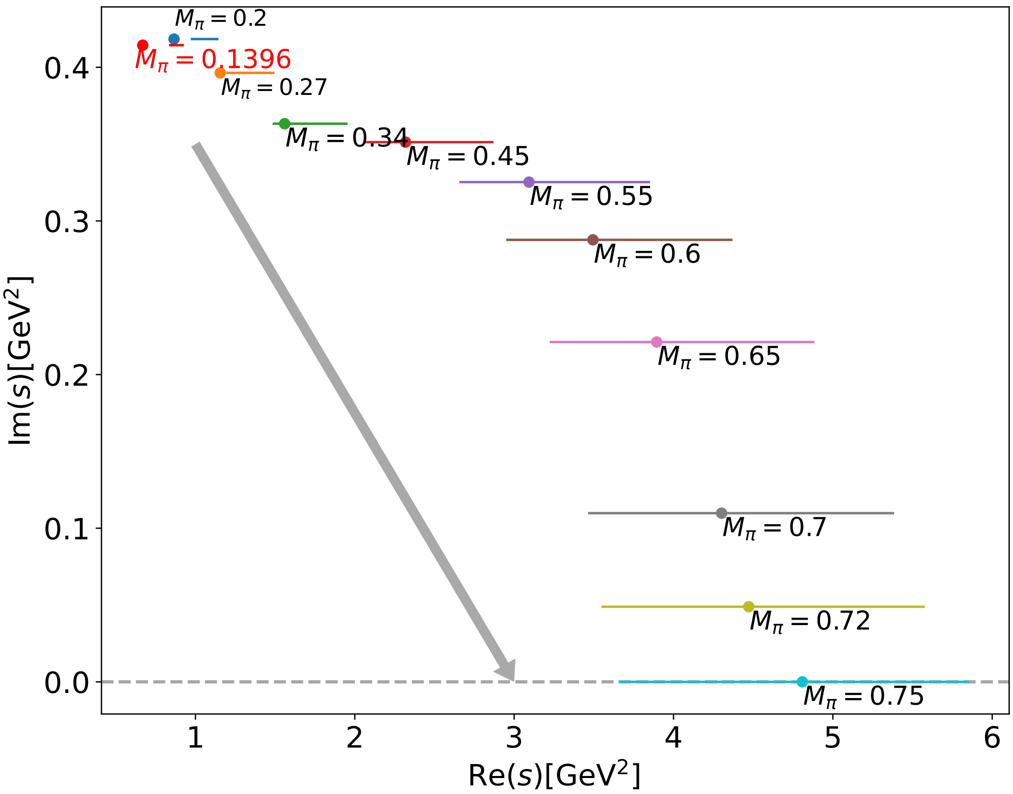

Figure 9: Trajectory of $N^*(920)$ pole in s-plane at $\mathcal{O}(p^3)$

we obtained qualitatively similar results for the quark-mass dependence of the $N^*(920)$ resonance in Fig. 9. This consistency across different low-energy constant choices demonstrates the robustness of our findings.

In addition to the tree-level calculations, we also computed the loop diagrams at $\mathcal{O}(p^3)$. The complete results, incorporating both tree-level and loop contributions, are presented in Fig. 10.

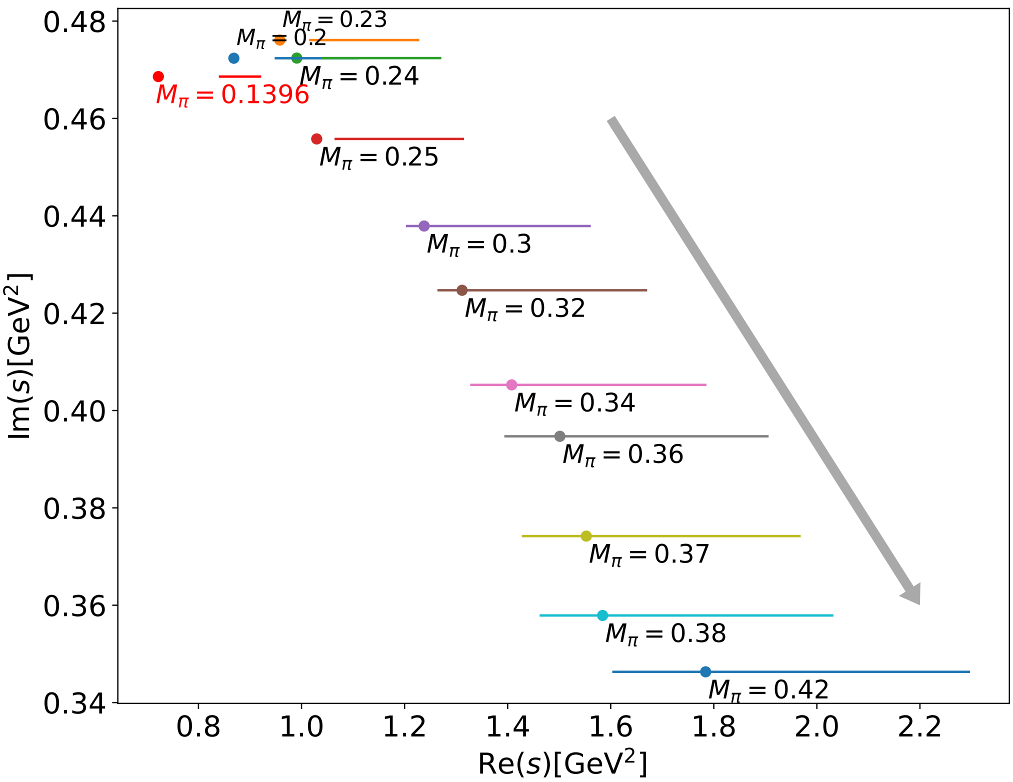

Figure 10: Full $\mathcal{O}(p^3)$ results including loop corrections.

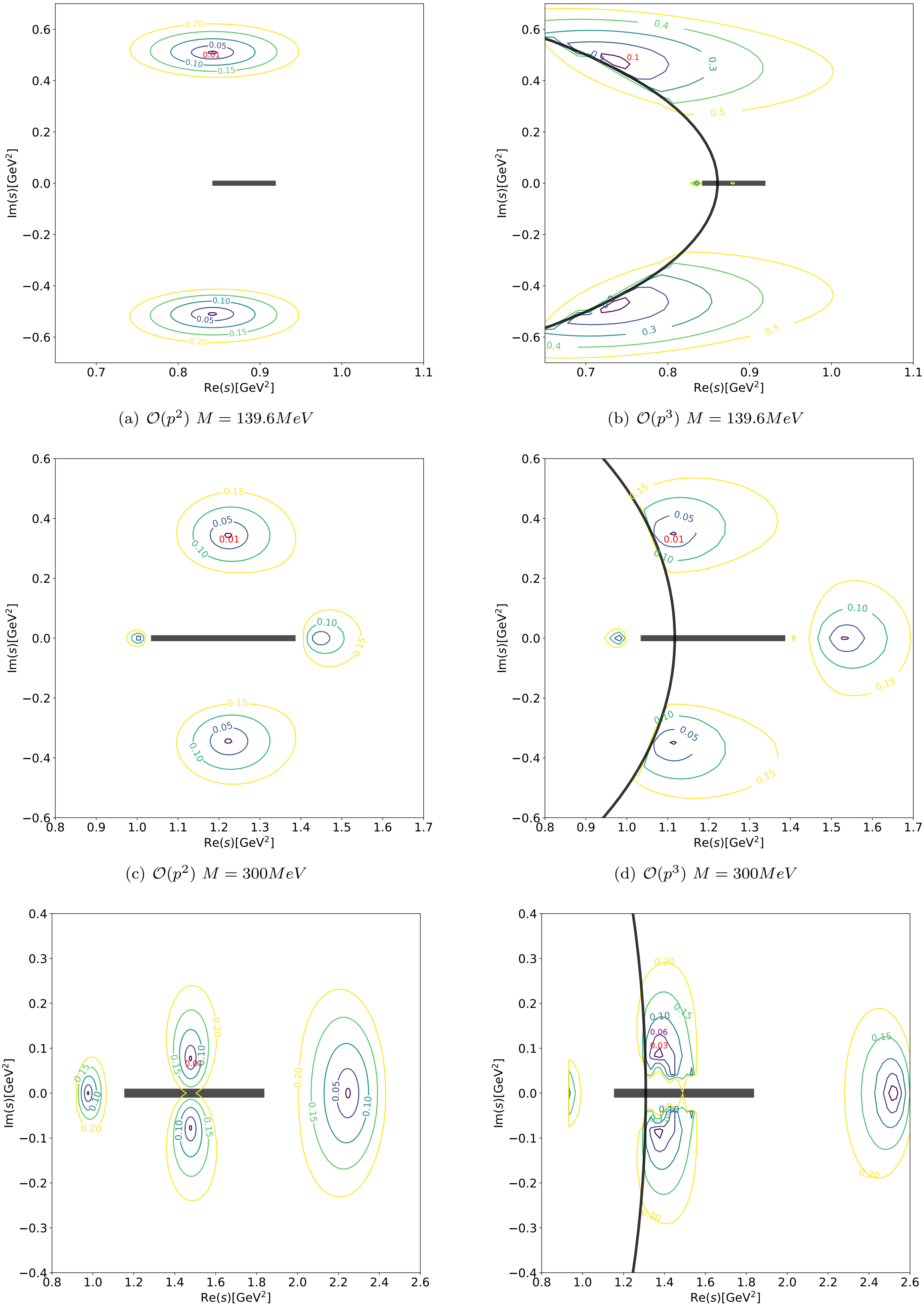

(a) $\mathcal{O}(p^2)$ $M = 139.6MeV$

(b) $\mathcal{O}(p^3)$ $M = 139.6MeV$

(c) $\mathcal{O}(p^2)$ $M = 300MeV$

(d) $\mathcal{O}(p^3)$ $M = 300MeV$

(e) $\mathcal{O}(p^2)$ $M = 420MeV$

(f) $\mathcal{O}(p^3)$ $M = 420MeV$

Figure 4: The contour of the modulus of the S_{11} matrix element on the first sheet of s plane. Thick black lines represent the cuts.